Journal of Applied Physics, Vol. 123, 2018, Article number 114501
DOI:10.1063/1.5018343

Cryogenic Scintillation Properties of *n*-Type GaAs for the Direct Detection of Sub-GeV/c^2 Dark Matter

S. Derenzo[a], E. Bourret[b], G. Bizarri[a], S. Hanrahan[a], and M. Pyle[c]

[a] Molecular Biophysics and Integrated Bioimaging Division, Lawrence Berkeley National Laboratory

[b] Materials Sciences Division, Lawrence Berkeley National Laboratory

[c] Physics Department, University of California, Berkeley

This paper describes the cryogenic scintillation properties of *n*-type GaAs for the detection of dark matter (DM) particles in the poorly explored mass range from 1 to 1000 MeV/c^2. Seven samples from two commercial suppliers with a variety of doping levels were studied. The optical excitation threshold is at the 1.52 eV bandgap and the emission band centered at 930 nm is due to the recombination of delocalized silicon donor electrons with boron acceptors. The X-ray excited luminosities at 10 K ranged from 7 to 43 photons/keV. Because our spectrometer did not measure wavelengths above 970 nm and an anti-reflective coating was not used, these values are underestimates. Future research in optimizing doping levels, growth conditions, and anti-reflective coatings should increase the luminosity toward the theoretical limit of 200 photons/keV. Thermally stimulated luminescence measurements showed that unlike NaI(Tl), NaI, and CsI scintillators, *n*-type GaAs doped above the Mott transition has conduction-band electrons that annihilate metastable radiative states that could cause afterglow. When used with cryogenic photodetectors this scintillator promises a remarkable combination of large target size, ultra-low backgrounds, and a sensitivity to electron recoils of a few eV that would be produced by DM particles as light as a few MeV/c^2.

Keywords: GaAs, scintillation, donor-acceptor emission, Mott transition, afterglow, dark matter, electron recoil.

Published by AIP. This is the Author Accepted Manuscript issued with:
Creative Commons Attribution Non-Commercial License (CC:BY:NC 4.0).
The final published version (version of record) is available online at DOI:10.1063/1.5018343.
Please refer to any applicable publisher terms of use.

I. INTRODUCTION

This paper presents the first measurements of GaAs as a scintillation radiation detector and is organized as follows: Background section II describes previous experiments to detect heavy (>1 GeV/c^2) dark matter particles and a new approach for detecting sub-GeV/c^2 DM particles through their interaction with electrons in a scintillator. Section III describes the GaAs crystal samples and the measurement equipment used. Section IV presents experimental results and discussions of optical emissions during optical and X-ray excitation, afterglow, and optical scattering. Section V estimates the radiogenic backgrounds. Section VI discusses the significance of this work for future DM searches and section VII lists the conclusions. Appendix A compares the maximum nuclear and electron recoil energies as a function of DM particle mass. Appendix B estimates the free carrier concentration at the Mott transition for silicon-doped *n*-type GaAs using previously published data.

II. BACKGROUND

Despite overwhelming evidence that large amounts of cold DM are gravitationally associated with galaxies and galactic clusters, recent large-scale experiments designed to detect nuclear recoils from DM particles with masses above 1 GeV/c^2 have not seen a definitive signal [1-6]. This has motivated designs for experiments that search for DM particles in the sub-GeV/c^2 range, using both electron and nuclear recoils. Sub-GeV/c^2 DM particles are expected to interact more efficiently with electrons than with nuclei [7-9]. For example, a DM particle with a mass of 5 MeV/c^2 and a typical velocity of 10^{-3} c has a kinetic energy of 2.5 eV, most of which can be transferred to a recoil electron and detected by low band gap detector materials. In contrast, the maximum energy that can be transferred by the same DM particle to a helium nucleus in an elastic collision is 0.012 eV, whose detection will require the use of ultra-low energy threshold

processes such as the evaporation and detection of helium atoms from super-fluid helium [10-12]. It is important to search for both electron and nuclear recoils since it is not known whether DM is leptophilic, hadrophilic, or both [13].

Since the rate of energetic electron recoils is strongly suppressed, even for DM masses as high as 1 GeV/c^2, detector materials with a low band gap are favored [9]. Scintillation detectors have an advantage over semiconductor ionization detectors (e.g. Ge) in that they do not require an electric field and afterglow from metastable radiative states is expected to be lower than dark currents [14]. This led to the choice of *n*-type GaAs for this work because of its low band gap (1.52 eV), donor-acceptor luminescence [15, 16], and the commercial production of large, high-quality crystals. It has not been previously reported as a scintillator for radiation detection.

Previous work on silicon-doped *n*-type GaAs at cryogenic temperatures attributed the emissions near 850 nm to transitions from shallow silicon donors to shallow acceptors [16-18], and the emissions near 930 nm to transitions from shallow silicon donors to the acceptor boron on an arsenic site [16, 19]. Additional emissions have been reported near 1,100 nm [20] and 1,250 nm [21] but these do not involve boron and are beyond the range of our spectrometer. See [16] for a recent summary of the experimentally observed emissions, [22] for a discussion of the defects introduced by silicon and boron, and [18] for first-principles computations of their defect levels.

Detection of single photons in the near infrared with high efficiency and low background at cryogenic temperatures is a challenge, but this technology is under active development using transition edge sensors [23] and microwave kinetic inductance detectors [24]. Another possibility is an optical absorber in superfluid helium. The heat from absorbed photons will produce

hundreds of phonons and quasi-particles that evaporate a corresponding number of helium atoms [12]. Anti-reflection coatings can be used reduce internal trapping of the scintillation light [25].

III. SAMPLES AND MEASUREMENT EQUIPMENT

A. GaAs Samples

Table I lists the samples used in the measurements. They are in the form of wafers with thicknesses from 0.35 to 0.60 mm. All samples have low electrical resistances at 10 K, consistent with doping above the Mott transition carrier concentration of 8×10^{15} free carriers cm^{-3} (see Appendix A). The *n*-type free carrier concentrations cannot be easily estimated from the silicon and boron dopant concentrations, since both can occupy gallium and arsenic sites.

Table I. GaAs samples used in this work. Si, B, and P concentrations determined by Glow Discharge Mass Spectrometry. Free carrier concentrations determined by Hall effect.

Sample number	Supplier	Si ppm(wt) atoms/cm^3	B ppm(wt) atoms/cm^3	P ppm(wt) atoms/cm^3	*n*-type free carriers/cm^3
13316	AXT[a]	8.9 1.02×10^{18}	9.7 2.87×10^{18}	0.008 8×10^{14}	5.5×10^{17}
13352	AXT[a]	7.7 8.8×10^{17}	11 3.3×10^{18}	0.006 6×10^{14}	b
13353	AXT[a]	7.2 8.2×10^{17}	9.2 2.73×10^{18}	0.003 3×10^{14}	b
13354	AXT[a]	7.3 8.3×10^{17}	12 3.6×10^{18}	0.005 5×10^{14}	b
13330	Freiberger[c]	8.3 9.5×10^{17}	5.2 1.54×10^{18}	2.8 2.9×10^{17}	6.02×10^{17}
13332	Freiberger[c]	14.6 1.67×10^{18}	6.8 2.02×10^{18}	5.2 5.4×10^{17}	1.44×10^{18}
13333	Freiberger[c]	20 2.3×10^{18}	7.9 2.34×10^{18}	4.4 4.6×10^{17}	2.03×10^{18}

[a]AXT, Inc. (Fremont, California)

[b]Not measured but expected to be similar to 13316 since Si and B are similar

[c]Freiberger, Inc. (Freiberg, Germany)

B. Cryostat

Samples were cooled with an ARS-2HW helium compressor and DE-202 two-stage cold finger (both from Advanced Research Systems, Macungie, PA). The temperature was regulated with a Model 336 controller (Lake Shore Cryotronics, Westerville, OH).

C. Optically-excited Luminescence

Optical excitation was provided by a Model XS433 Xe broad spectrum lamp coupled to a Model SP2150i double grating monochromator (both from Acton Research Corp., Acton, MA). A split optical fiber sent light from the monochromator to the sample and to a silicon reference photodiode. The photodiode was used to calibrate the excitation monochromator for lamp aging and for the wavelength-dependent combined output of the lamp, grating, and optical fiber. Fluorescence spectra were measured using a double-grating SpectraPro-2150i spectrometer with order-sorting filter wheel and a PIXIS:100B thermoelectrically cooled charge coupled detector (silicon CCD) (both from Princeton Instruments, Inc., Trenton, NJ). A white Teflon reflector was used to calibrate the emission spectrometer for wavelength variations in the combined response of the gratings, filters, and CCD. Samples were cooled using the cryostat described in section B.

D. X-ray-excited Luminescence and Afterglow

The X-ray beam was produced by a Nonius FR591 water-cooled rotating copper-anode X-ray generator (50 kV, 60 mA) (Bruker AXS Inc., Madison, WI). The X-ray excited emission spectra, afterglow, and thermally stimulated emissions were measured using this system, the emission spectrometer described in the section C, and the cryostat described in section B.

E. Optical Transmission

The optical transmission source was a TMc300V-QC triple grating IR monochromator with 100W quartz-halogen lamp and order-sorting filter wheel (Bentham Instruments, LTD, Berkshire, UK). The optical power transmitted through the GaAs samples was measured using a PMD100D optical power meter (Thorlabs Inc. Newton, NJ).

IV. RESULTS AND DISCUSSION

A. Optical excitation

Figure 1 shows the emission spectrum of sample #13316 at 10K as a function of optical excitation wavelength. A very weak emission band peaking at 850 nm (1.46 eV) and a much stronger emission band peaking at 930 nm (1.33 eV) are observed.

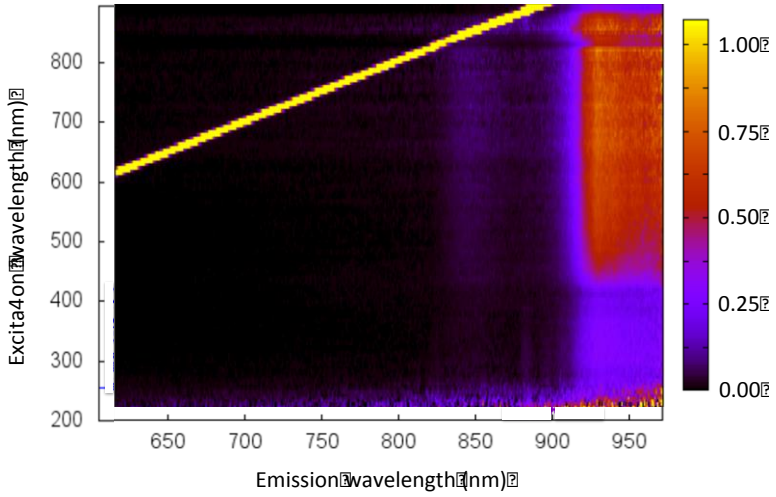


Figure 1. Emission spectrum as a function of excitation wavelength for sample #13316 at 10K.

Figure 2 shows the optical excitation and emission curves for sample #13316 at 10K. The excitation peak at 815 nm (1.52 eV) corresponds to the excitation of valence band electrons to the conduction band (Figure 3 left). The excitation peak at 860 nm (1.44 eV) corresponds to the excitation of boron acceptor electrons to the conduction band (Figure 3 right). The Stokes shift between the excitation and emission peaks is 0.11 eV. Wavelengths longer than 970 nm were not recorded by the spectrometer.

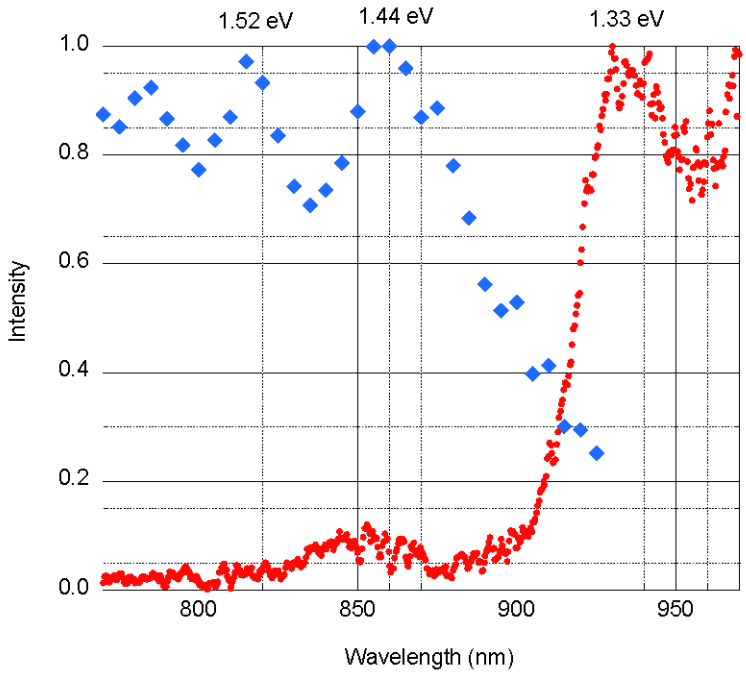


Figure 2. Sample #13316 optical excitation curve for 955 nm emission, and emission curve for 750 nm excitation at 10K.

Figure 3 shows a simplified diagram of the excitation and emission processes. In the ground state of *n*-type GaAs the Fermi (highest occupied) level is at the conduction band minimum and all boron acceptor sites are electron saturated. Figure 3 left: (1) A photon promotes a valence band electron into the conduction band, (2) the valence band hole is filled by a boron electron, which transfers the hole to the boron, (3) the change in charge of the boron atom causes a lattice relaxation, (4) a donor electron combines with the boron hole, producing a 1.33 eV photon. It is possible that the radiative center is an exciton containing a weakly bound electron. Figure 3 right: (1) A photon promotes a boron electron into the conduction band followed by the previous processes (3) and (4). Not shown are mid-gap electron traps (e.g. EL2) that cause non-radiative recombination. As described in [22] boron can replace gallium as an isoelectronic substitution or replace arsenic as an acceptor.

The silicon donor ionization energy in GaAs is 5.8 meV. As a result, in *n*-type GaAs at room temperature (k*T* = 25 meV) some of the silicon donor electrons are bound to boron acceptors and the remainder are distributed nearly equally between silicon atoms and the conduction band. The free carrier concentration for *n*-type GaAs is measured and reported under these conditions. On cooling to 0 K free carriers below the Mott limit bind to silicon atoms and the rest remain in the conduction band. As a result, the concentration of free carriers at 0K is equal to the free carrier concentration at room temperature minus the Mott limit concentration (see Appendix B).

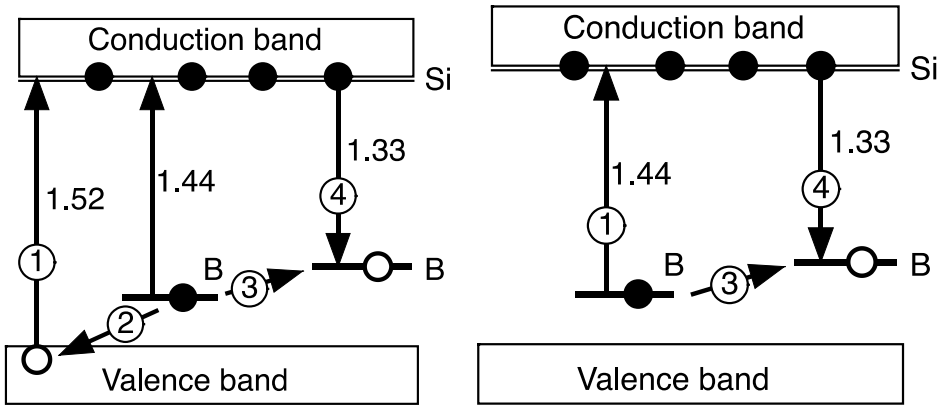


Figure 3. Simplified diagram of excitation and emission processes. Energy units in eV. See text for details.

B. X-ray Excitation

Figure 4 shows the emission spectrum of sample #13316 when excited with 50 keVp X-rays at 10 K. The X-ray excited 930 nm emission band is almost identical to the optically-excited emission band in Figure 2. The observed luminosity was estimated to be about 43 photons/keV by calibrating against standard $Bi_4Ge_3O_{12}$ and Lu_2SiO_5:Ce scintillation crystals of equal size. This is an underestimate because (1) it does not include emissions above 970 nm and (2) the higher refractive index of GaAs (3.55) results in more internal trapping than the standards.

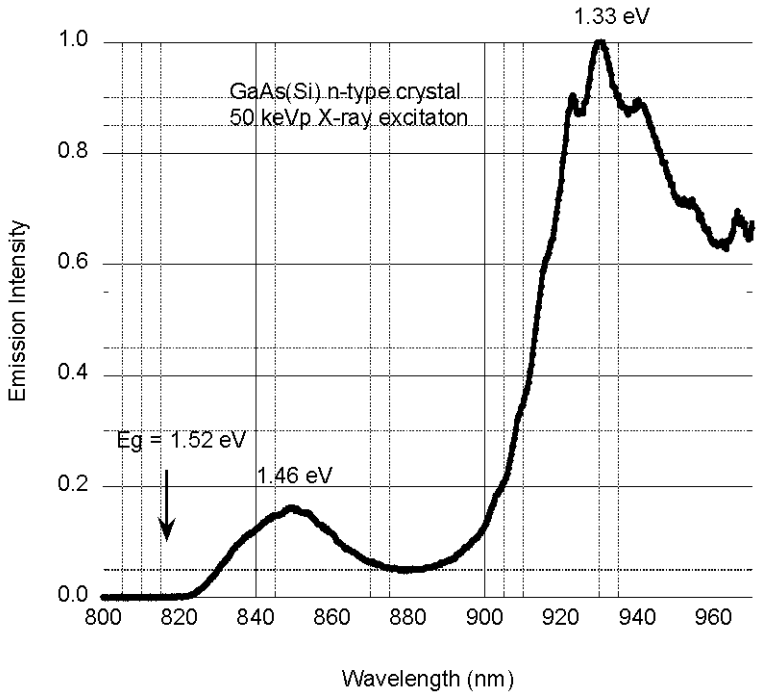


Figure 4. X-ray excited emission spectrum of sample #13316 at 10K

Figure 5 shows the thermal quenching of the 850 nm and 930 nm emission peaks during 50 keVp X-ray excitation. The 850-nm emission is due to the recombination of shallow donor electrons with holes trapped on shallow acceptors [16-18]. These shallow states are quenched above 20 K with an activation energy of about 4.3 meV. The 930 nm emission is due to the recombination of donor electrons with holes trapped on boron acceptors [16, 26] at a depth of 188 meV [19]. This deeper state is quenched at 120 K with an activation energy of about 12 meV. We conclude that this value is the thermal barrier for the transfer of the hole from the boron acceptor to deeper (e.g. EL2) traps.

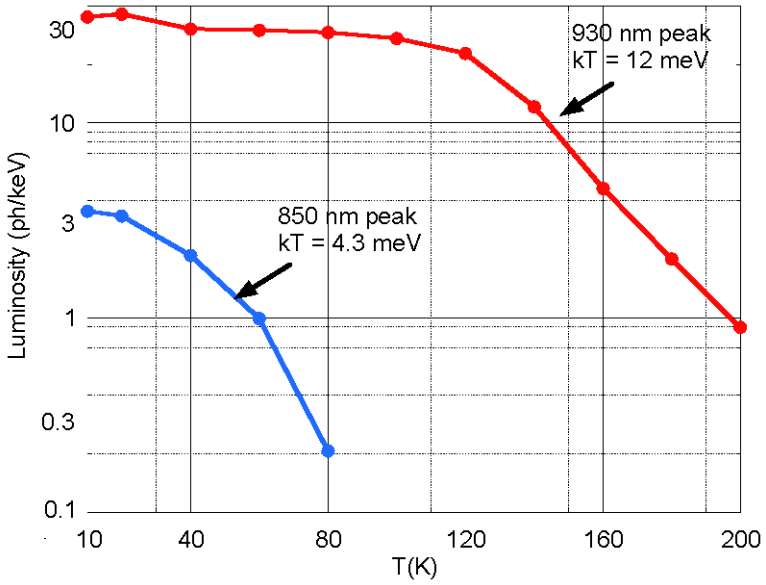


Figure 5 Luminosity of sample #13316 in the 930 nm (upper curve) and 850 nm (lower curve) emission peaks during 50 keVp X-ray excitation as a function of temperature.

Table II lists the X-ray excited luminosity for the seven samples used in this work. While there is a weak correlation between doping levels and total luminosity of the AXT and the Freiberger samples taken separately, the primary difference is that the AXT samples are about five times more luminous than the Freiberger samples. The relative low total luminosity of the Freiberger set could be due to a deep (e.g. EL2) native impurity level that is more efficient than boron in trapping holes, or could be due to the higher concentration of phosphorous. In the Freiberger set the emission shifts from 930 nm to 850 nm as the free carrier concentration is increased (e.g. sample 13330 vs. 13333). This indicates an increased involvement of shallow acceptor defects as the silicon concentration is increased. In a large crystal, an 850-nm photon would be absorbed and re-emitted into the 930-nm band (Figure 2).

Table II. 10K. Scintillation properties of six samples at 10K.

Sample number	Supplier	Luminosity (photons/MeV)	Fraction @850 nm	Fraction @930 nm
13316	AXT	43,000	0.08	0.92
13352	AXT	39,000	0.05	0.95
13353	AXT	33,000	0.08	0.92
13354	AXT	31,500	0.08	0.92
13330	Freiberger	7,000	0.33	0.67
13332	Freiberger	8,900	0.55	0.45
13333	Freiberger	9,500	0.85	0.15

C. AFTERGLOW

Figure 6 shows the scintillation intensity of sample #13330 at 10K in 2s time steps before, during, and after exposure to the 50 keVp X-ray beam. The beam shutter was manually opened from 300s to 900s. Since the closing of the X-ray shutter was not synchronized with the data acquisition, the point at 900 s could be an instrumental artifact.

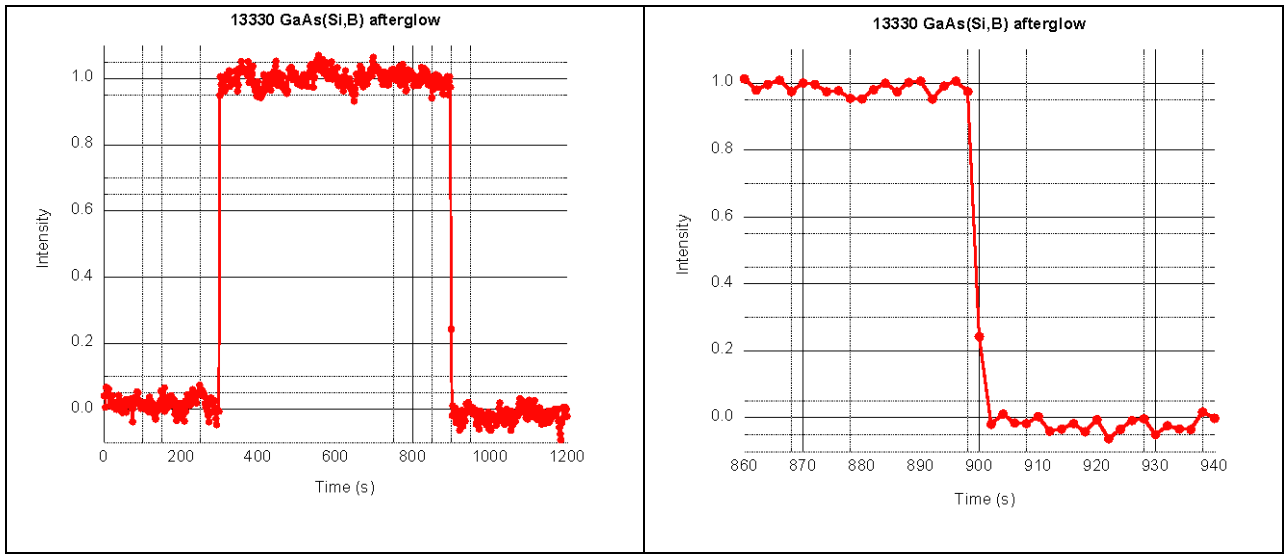


Figure 6. Left: emission before, during, and after exposure to a 50 keVp X-ray beam, measured in 2s time bins. Right: enlargement of emission around the time the beam was turned off.

D. THERMALLY STIMULATED EMISSION

Figure 7 shows the thermally stimulated luminescence from sample #13330 and crystals of Nai(Tl), NaI, and CsI of similar size. The crystals were first excited with a 50 keVp X-ray beam for 30 minutes at 10K and then the emissions were recorded as the temperature was increased to 300 K over a period of 50 minutes. The emission peaks appear at temperatures characteristic of the trap depths of metastable excited states. If the temperature were held at 10 K after excitation these same traps would slowly release to produce an afterglow background as the system returned to its ground state. Figure 8 shows that the GaAs emission curve is essentially the same as the instrumental background. These results show that in a DM experiment background high-energy ionization events from muons and gamma rays will not result in an accumulation of metastable radiative states that could cause afterglow.

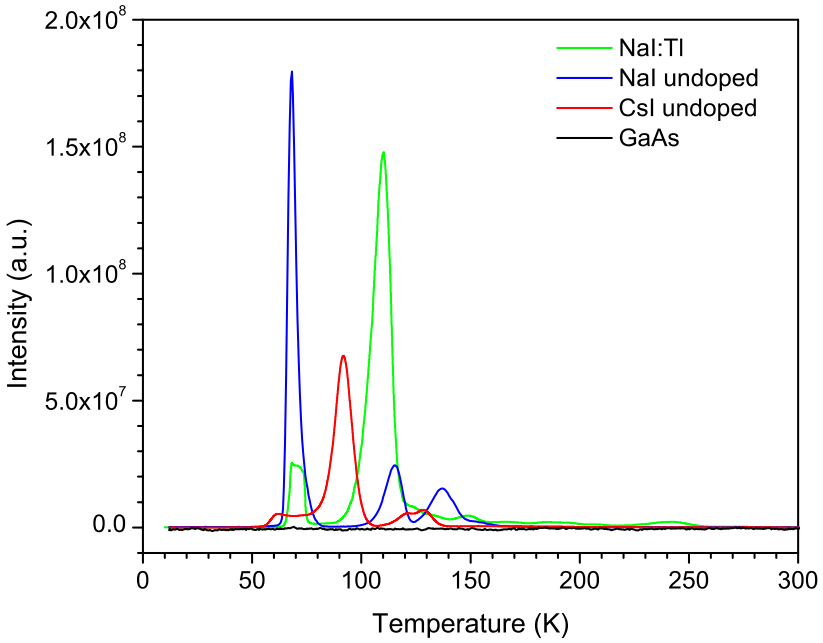


Figure 7. Thermally stimulated luminescence of GaAs sample #13330 and crystals of NaI(Tl), NaI, and CsI as a function of temperature after a 30-minute exposure to a 50 keVp X-ray beam at 10K. All crystals were similar in size. The vertical scale is the same for all samples. See Figure 8 for a comparison between the GaAs curve and the instrumental background.

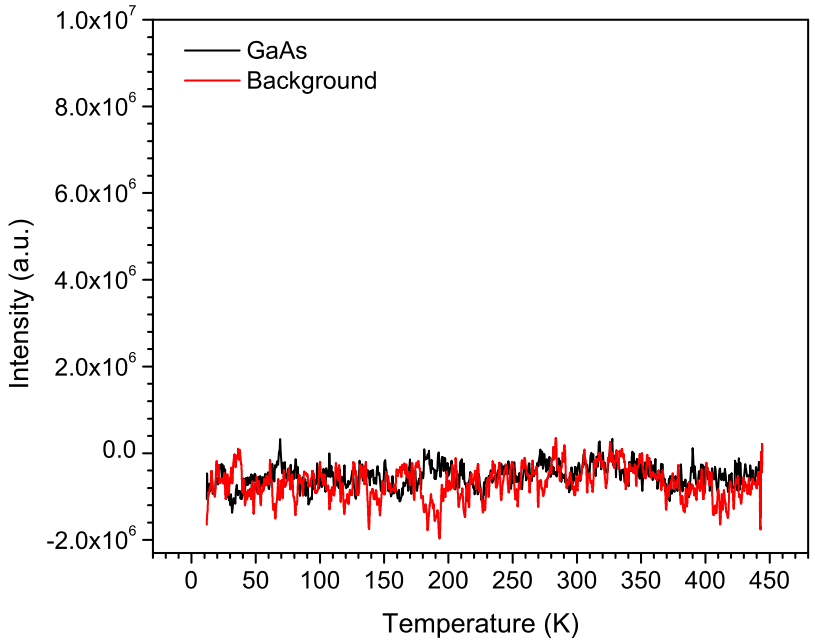


Figure 8. Comparison between the GaAs thermally stimulated emission in Figure 7 and the instrumental background. Both curves have a slight instrumental offset. Note that the vertical scale has been enlarged 20x relative to Figure 4.

D. Optical scattering from conduction band electrons

Scattering of optical photons by conduction band electrons in *n*-type GaAs has been measured with free carrier concentrations from 2 x 10^{17} to 6.7 x 10^{18} per cm^3 [27]. Unfortunately, these data only cover exponential attenuation factors greater than 10/cm and for wavelengths close to the band gap. To estimate the scattering of photons with energies below the band gap we measured the optical transmission of samples 13330, 13332, and 13333 from 0.6 to 1.2 eV (from 0.8 to 0.2 eV below the room temperature band gap). The transmission is essentially constant over this energy range and the average values are listed in Table III. Table III also lists the free carrier concentrations *n*, thicknesses *Z*, 2D projected carrier concentrations *nZ*, and average transmissions of samples 13330, 13332, and 13333. The best mono-exponential fit to the

transmission data was 0.390 exp(-nZ/1.85 x 10^{17}/cm^2) with an rms = 0.008. In this model the scattering length is 18.5 cm at a carrier concentration of 1 x 10^{16}/cm^3. All samples had one polished surface and one ground surface, and all were assumed to have the same Fresnel reflection and surface scattering loss. These factors result in a transmission of 0.390 at $nZ = 0$ which can be increased using anti-reflective coatings.

Table III. Optical transmission properties of three samples at room temperature

Sample number	Supplier	*n* in carriers/cm^3	Thickness Z (mm)	nZ in carriers/cm^2	Optical transmission
13330	Freiberger	6.02 x 10^{17}	0.577	3.47 x 10^{16}	0.322
13332	Freiberger	1.44 x 10^{18}	0.548	7.89 x 10^{16}	0.259
13333	Freiberger	2.03 x 10^{18}	0.549	1.11 x 10^{17}	0.201

V. RADIOGENIC BACKGROUNDS

The longest-lived radioactive isotope of gallium is ^{67}Ga, which has a half-life of 3.3 days and decays by electron capture to the stable isotope ^{67}Zn. The longest-lived radioactive isotope of arsenic is ^{73}As, which has a half-life of 80 days and decays by electron capture to the stable isotope ^{73}Ge.

Glow discharge mass spectrometry of the four AXT samples found that the weight fractions for the chemical elements that contain primordial radioactive contaminants (K, Rb, La, and Lu) were all below 0.5 ppb. The highest potential beta particle background is from the radioactive isotope ^{87}Rb, which has a 28% abundance and a 4.9 x 10^{10} year half-life. An atomic impurity fraction of 0.5 wt ppb Rb in 1 kg of GaAs contains 1 x 10^{15} atoms of ^{87}Rb, which decay at the rate of 1.4 x 10^4 yr^{-1}. The beta end point is 283 keV and the low end of the beta spectrum will

contain about 0.1 betas kg^{-1} eV^{-1} yr^{-1}. The corresponding beta background from 0.5 ppb of K is about 10^{-3} kg^{-1} eV^{-1} yr^{-1}. The corresponding beta background from 0.5 ppb of La is about 3×10^{-5} kg^{-1} eV^{-1} yr^{-1}. The corresponding beta background from 0.5 ppb of Lu is about 3×10^{-3} kg^{-1} eV^{-1} yr^{-1}. Since a ^{87}Rb background was not reported in DM searches that use large volumes of NaI(Tl) [1], we conclude that Rb impurities can be reduced to levels well below 0.5 ppb.

VI. DISCUSSION

These measurements show that *n*-type GaAs is a promising cryogenic scintillator for DM particle detection in the MeV mass range in that it can be grown as large, high-quality crystals, has good scintillation luminosity, a threshold sensitivity at the 1.52 eV bandgap, and potentially no afterglow. However, more work is needed to optimize the doping concentrations, to reduce hole traps that compete with boron acceptors, and to develop anti-reflective coatings and cryogenic photodetectors. The *n*-type free carrier concentration must be high enough to efficiently combine with the boron acceptors and metastable radiative states but not so high as to introduce an unacceptable level of optical scattering and Auger quenching.

GaAs does not have an advantage over current techniques for detecting DM particles in the GeV/c^2 mass range because the maximum nuclear and electron recoil energies are similar (see Appendix A) and liquid xenon targets can be made much more massive.

VII. CONCLUSIONS

1) Electron excitations 1.44 eV and above can produce 1.33 eV photons.
2) The scintillation emission band from X-ray excitation peaks at 1.3 eV (930 nm) and is due to the transition of electrons from silicon donors to boron acceptors.

3) The most luminous GaAs sample studied (#13316) has an observed scintillation luminosity of 43 photons/keV, below the theoretical limit of 200 photons/keV. The limiting factor appears to be undesired hole traps that compete with the boron acceptors.
4) Ionization from background radiation (e.g. muons and gamma rays) is not expected to cause afterglow, provided that the free carrier concentration is above the Mott transition, where the conduction band electrons annihilate any metastable radiative states
5) At a free carrier concentration of $1 \times 10^{16}/cm^3$ (near the Mott limit), the scattering length for optical photons is about 18 cm.

Acknowledgements

We thank A. Canning, R. Essig, A. Massari, A. Soto, T.-T. Yu, and R. Williams for helpful discussions, T. Shalapska for assistance in data analysis, G. Martens for help in locating literature data, and Freiberger, Inc. for providing GaAs samples. This work was supported in part by the Office of Basic Energy Sciences of the U.S. Department of energy, in part by Advanced Crystal Technologies. Inc. of Knoxville, TN, and carried out using facilities provided by the U.S. Department of Homeland Security, Domestic Nuclear Detection Office at the Lawrence Berkeley National Laboratory under UC-DOE Contract No. DE-AC02-05CH11231.

Appendix A: Maximum electron and nuclear recoil energies as a function of DM particle mass.

Figure A shows the maximum nuclear and electron recoil energies as a function of DM particle mass at a velocity $v = 10^{-3}\ c$, which is about one-half the galactic escape velocity. The maximum nuclear recoil energy is $2 \times 10^{-6}\ c^2\ (M_D^2\ M_N)/(M_D + M_N)^2$, where M_N is the nucleus

mass and M_D is the DM particle mass. The maximum electron recoil energy is equal to the kinetic energy of the DM particle, $0.5 \times 10^{-6}\ c^2\ M_D$.

Using electron recoils in a detector with an energy threshold of 1.5 eV, DM particle masses as low as 3 MeV can be reached. For the same low mass reach using nuclear recoils ultra-low threshold (~meV) techniques are needed, such as the evaporation and detection of helium atoms from superfluid helium at mK temperatures [12].

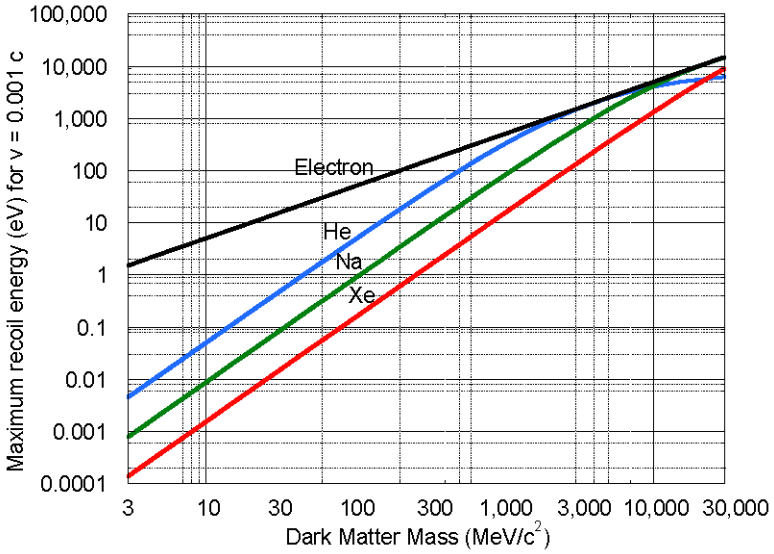


Figure A. Maximum nuclear and electron recoil energy as a function of DM particle mass, assuming a velocity of $10^{-3}\ c$.

Appendix B: The Mott transition in silicon-doped *n*-type GaAs

Figure B plots the electrical conductivity at 0 K of silicon-doped *n*-type GaAs as a function of the free carrier concentration measured at 300 K. The data are 0 K extrapolations taken from [28]. The conductivity is zero below $8 \times 10^{15}\ cm^3$ (the Mott transition) and rises linearly above that value. Below the Mott transition concentration, cooling from room temperature to 0K causes the free carriers to become bound to individual silicon atoms at an energy level 5.8 meV below the conduction band minimum and they do not contribute to the electrical conductivity. Above

the Mott transition concentration, cooling to 0 K results in a "metallic" state because mutual repulsion forces the additional electrons into the next higher available energy level, which is at the conduction band minimum. At 0 K only the electrons forced into the conduction band contribute to the electrical conductivity and their concentration is equal to the room temperature carrier concentration minus the Mott transition concentration.

Exceeding the Mott transition is important for scintillation at 0K because it provides highly mobile conduction band electrons that can efficiently combine with ionization holes trapped anywhere in the gap. This serves to maximize the prompt radiative emission (the desired signal), and annihilate metastable radiative states that could cause unwanted afterglow. However, an excessive free carrier concentration is not desirable because of increased optical scattering and Auger quenching.

It is interesting to note that both the donor ionization energy (5.8 meV) and Mott transition concentration ($8 \times 10^{15}/cm^3$) are uniquely low for GaAs(Si). For example, these values are 13 meV and 3.5×10^{17} for Ge(As) [29]; 30 meV and $2 \times 10^{18}/cm^3$ for CdS(Cl) [30]; and 45 meV and $3.7 \times 10^{18}/cm^3$ for Si(P) [31].

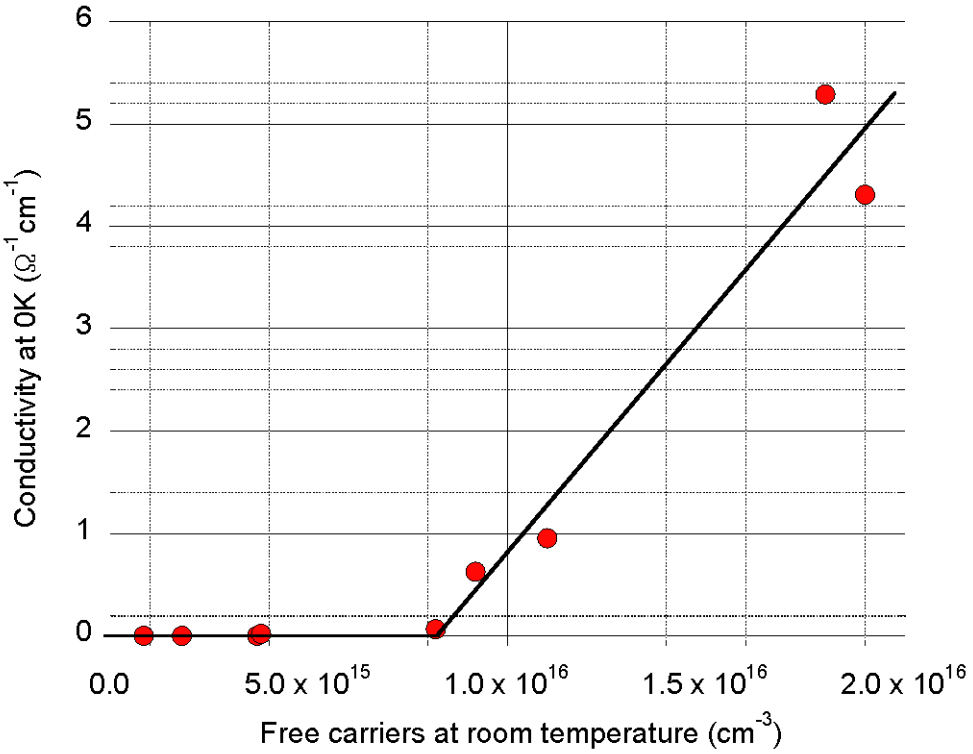


Figure 2. Electrical conductivity at 0K as a function of the free carrier concentration at 300K. When the room temperature free carrier concentration is below 8 x 10^{15} cm^{-3} (the Mott limit), cooling to 0K causes the carriers to be bound to their silicon donor atoms (i.e. they are "frozen out") and the electrical conductivity is zero. Above the Mott limit, additional free carriers populate the conduction band and the electrical conductivity rises in proportion to their concentration. (Data from [28])

References

[1] R. Bernabei *et al.*, "Final model independent results of DAMA/LIBRA-phase1 and perspectives of phase2," (in English), *Physics of Particles and Nuclei,* vol. 46, no. 2, pp. 138-146, Mar 2015.

[2] G. Angloher *et al.*, "Results on light dark matter particles with a low-threshold CRESST-II detector," *ArXiv Astrophysics e-prints,* vol. 1509.01515, 2016.

[3] E. Aprile *et al.*, "XENON100 dark matter results from a combination of 477 live days," (in English), *Physical Review D,* vol. 94, no. 12, Dec 12 2016.

[4] Agnese and e. al, "Results from the Super Cryogenic Dark Matter Search (SuperCDMS) experiment at Soudan," *ArXiv Astrophysics e-prints,* vol. 1708.08869, 2017.

[5] E. Aprile *et al.*, "First Dark Matter Search Results from the XENON1T Experiment," *ArXiv Astrophysics e-prints,* vol. 1705.06655, 2017.

[6] D. S. Akerib *et al.*, "Results from a Search for Dark Matter in the Complete LUX Exposure," (in English), *Physical Review Letters,* vol. 118, no. 2, Jan 11 2017.

[7] R. Essig, A. Manalaysay, J. Mardon, P. Sorensen, and T. Volansky, "First Direct Detection Limits on Sub-GeV Dark Matter from XENON10," (in English), *Physical Review Letters,* vol. 109, no. 2, Jul 12 2012.

[8] R. Essig, J. Mardon, and T. Volansky, "Direct detection of sub-GeV dark matter," (in English), *Physical Review D,* vol. 85, no. 7, Apr 9 2012.

[9] R. Essig, M. Fernandez-Serra, J. Mardon, A. Soto, T. Volansky, and T. T. Yu, "Direct detection of sub-GeV dark matter with semiconductor targets," (in English), *Journal of High Energy Physics,* no. 5, May 9 2016.

[10] K. Schutz and K. M. Zurek, "Detectability of Light Dark Matter with Superfluid Helium," (in English), *Physical Review Letters,* vol. 117, no. 12, Sep 14 2016.

[11] S. Knapen, T. Y. Lin, and K. M. Zurek, "Light dark matter in superfluid helium: Detection with multi-excitation production," (in English), *Physical Review D,* vol. 95, no. 5, Mar 22 2017.

[12] H. J. Maris, G. M. Seidel, and D. Stein, "Dark Matter Detection Using Helium Evaporation and Field Ionization," *ArXiv Astrophysics e-prints,* p. 1706.00117, 2017.

[13] S. Knapen, T. Lin, and K. M. Zurek, "Light Dark Matter: Models and Constraints," *ArXiv Astrophysics e-prints,* vol. 1709.07882, pp. 1-44, 2017.

[14] S. Derenzo, R. Essig, A. Massari, A. a. Soto, and T.-T. Yu, "Direct Detection of sub-GeV Dark Matter with Scintillating Targets (arXiv:1607.01009)," *Phys. Rev. D,* vol. 96, p. 016026, 2017.

[15] D. A. Cusano, "Radiative Recombination from Gaas Directly Excited by Electron Beams," (in English), *Solid State Communications,* vol. 2, no. 11, pp. 353-358, 1964.

[16] V. Bondarenko, "Positron annihilation study of equilibrium point defects in GaAs (Chapter 4)," PhD Thesis, Mathematisch-Naturwissenschaftlich-Technischen Fakultät, Martin-Luther-Universität Halle-Wittenberg, 2003.

[17] D. J. Ashen, P. J. Dean, D. T. J. Hurle, J. B. Mullin, and A. M. White, "Incorporation and Characterization of Acceptors in Epitaxial GaAs," (in English), *Journal of Physics and Chemistry of Solids,* vol. 36, no. 10, pp. 1041-1053, 1975.

[18] R. Leitsmann *et al.*, "Boron-Silicon complex defects in GaAs: An ab initio study," (in English), *Journal of Applied Physics,* vol. 109, no. 6, Mar 15 2011.
[19] S. K. Brierley, H. T. Hendriks, W. E. Hoke, P. J. Lemonias, and D. G. Weir, "Observation of Boron-Related Photoluminescence in GaAs-Layers Grown by Molecular-Beam Epitaxy," (in English), *Applied Physics Letters,* vol. 63, no. 6, pp. 812-814, Aug 9 1993.
[20] E. W. Williams, "Evidence for Self-Activated Luminescence in GaAs: The Gallium Vacancy-Donor Center," *Physical Review,* vol. 168, pp. 922-928, 1968.
[21] H. Lei, H. S. Leipner, V. Bondarenko, and J. Schreiber, "Identification of the 0.95 eV luminescence band in n-type GaAs : Si," (in English), *Journal of Physics-Condensed Matter,* vol. 16, no. 2, pp. S279-S285, Jan 21 2004.
[22] U. Kretzer, F. Boner, T. Bunger, and S. Eichler, "Influence of boron on the point defect equilibrium in highly n-doped gallium arsenide single crystals," (in English), *Physica B-Condensed Matter,* vol. 401, pp. 246-249, Dec 15 2007.
[23] T. Gerrits, A. Lita, B. Calkins, and S. W. Nam, "Superconducting Transition Edge Sensors for Quantum Optics (Chapter 2)," in *Superconducting devices in quantum optics*, R. H. Hatfield and G. Johnson, Eds. Switzerland: Springer International Publishing, 2016, pp. 31-60.
[24] P. Szypryt *et al.*, "High quality factor platinum silicide microwave kinetic inductance detectors," (in English), *Applied Physics Letters,* vol. 109, no. 15, Oct 10 2016.
[25] J. C. Zhang, L. M. Xiong, M. Fang, and H. B. He, "Wide-angle and broadband graded-refractive-index antireflection coatings," (in English), *Chinese Physics B,* vol. 22, no. 4, Apr 2013.
[26] H. Lei, H. S. Leipner, N. Engler, and J. Schreiber, "Interactions of point defects with dislocations in n-type silicon-doped GaAs," *J. Phys.: Condens. Matter,* vol. 14, pp. 7963-7971, 2002.
[27] H. C. Casey, D. D. Sell, and K. W. Wecht, "Concentration-Dependence of Absorption-Coefficient for n-type and p-type GaAs between 1.3 and 1.6 eV," (in English), *Journal of Applied Physics,* vol. 46, no. 1, pp. 250-257, 1975.
[28] M. Benzaquen, D. Walsh, and K. Mazuruk, "Conductivity of N-Type Gaas near the Mott Transition," (in English), *Physical Review B,* vol. 36, no. 9, pp. 4748-4753, Sep 15 1987.
[29] M. N. Alexander and D. F. Holcomb, "Semiconductor-to-Metal Transition in n-Type Group 4 Semiconductors," (in English), *Reviews of Modern Physics,* vol. 40, no. 4, pp. 815-+, 1968.
[30] S. Geschwind, R. Romestain, and G. E. Devlin, "Study of the Mott Transition in n-Type CdS by Spin Flip Raman Scattering and Spin Faraday Rotation," *Journal de Physique,* vol. C4-37, pp. 313-316, 1968.
[31] D. Jerome, C. Ryter, H. J. Schulz, and J. Friedel, "Si-P Revisited Electronic-Structure Observed by Magnetic-Resonance," (in English), *Philosophical Magazine B-Physics of Condensed Matter Statistical Mechanics Electronic Optical and Magnetic Properties,* vol. 52, no. 3, pp. 403-417, 1985.



https://dspace.org/

Cryogenic scintillation properties of n-type GaAs for the direct detection of MeV/c2 dark matter

Derenzo, S.; Bourret, Edith D.; Hanrahan, S.; Bizarri, Gregory

2018-03-20
American Institute of Physics (AIP)
http://dx.doi.org/10.1063/1.5018343
Derenzo S, Bourret E, Hanrahan S, Bizarri G, Cryogenic scintillation properties of n -type GaAs for the direct detection of MeV/c2 dark matter, Journal of Applied Physics, Volume 123, Issue 11, 2018, Article number 114501

Downloaded from a DSpace repository. https://dspace.org/